Solar Energy Vol. 39, No. 3, pp. 221–231, 1987
Printed in the U.S.A.

0038-092X/87 $3.00 + .00

A NEW SIMPLIFIED VERSION OF THE PEREZ DIFFUSE IRRADIANCE MODEL FOR TILTED SURFACES

RICHARD PEREZ† and ROBERT SEALS
Atmospheric Sciences Research Center, SUNY at Albany, Albany, NY 12222, U.S.A.

PIERRE INEICHEN†
Universite de Geneve, Groupe de Physique Appliquee, Geneve 4, CH-1211 Switzerland

RONALD STEWART†
Atmospheric Sciences Research Center, SUNY at Albany, Albany, NY 12222, U.S.A.

DAVID MENICUCCI
Sandia National Laboratories, Albuquerque, NM 87185, U.S.A.

Abstract—A new, more accurate and considerably simpler version of the Perez[1] diffuse irradiance model is presented. This model is one of those used currently to estimate short time step (hourly or less) irradiance on tilted planes based on global and direct (or diffuse) irradiance. It has been shown to perform more accurately than other models for a large number of locations worldwide. The key assumptions defining the model remain basically unchanged. These include (1) a description of the sky dome featuring a circumsolar zone and horizon zone superimposed over an isotropic background, and (2) a parameterization of insolation conditions (based on available inputs to the model), determining the value of the radiant power originating from these two zones. Operational modifications performed on the model are presented in a step by step approach. Each change is justified on the basis of increased ease of use and/or overall accuracy. Two years of hourly data on tilted planes from two climatically distinct sites in France are used to verify performance accuracy. The isotropic, Hay and Klucher models are used as reference. Major changes include (1) the simplification of the governing equation by use of reduced brightness coefficients; (2) the allowance for negative coefficients; (3) reduction of the horizon band to an arc-of-great-circle; (4) optimization of the circumsolar region width; and (5) optimization of insolation conditions parameterization.

1. INTRODUCTION

It is a current practice, for evaluating the energy received by a tilted surface, to decompose the solar radiation into three components which are treated independently[1]: Direct beam, sky diffuse and ground-reflected.

Models differ generally in their treatment of the sky diffuse component which is considered as the largest potential source of computational error[2]. While the treatment of the direct component is straightforward and virtually error-free for flat surfaces, that of the ground reflected component may also be a cause of computational errors which are in most instances, however, of lesser overall impact than that caused by a poor description of the sky hemisphere.

In a separate paper, the authors investigate this last point and describe simple guidelines to account adequately for the ground reflected component[3]. The model discussed in this paper focuses on the treatment of the sky diffuse component.

Originally developed to handle instantaneous events[1, 4], the Perez model, as it has become to be known, has been more extensively used for hourly applications. Although it requires no more input than the most simple model assuming isotropic sky[5], i.e. global and direct or diffuse irradiance, it has been found to perform substantially better than that as well as other widely used anisotropic models [e.g. 6–8] when tested against independent data sets [e.g. 9–12].

The model was recently incorporated into Sandia National Laboratories' (SNL) photovoltaic simulation program, PVFORM[13]. However, more widespread application of this model has been subject to question because of (1) the fact that it was quite more complex to use than other models and (2) the fact that it had not yet been validated for an extended set of environments.

The first point is addressed to a large extent in this paper: A new simpler and slightly higher performance, version of the model is presented.

The second of these concerns is being addressed by Sandia National Labs who currently conducts an extensive measurement program geared to validate and/or configure the model for different key climatic environments[14]. The impacts of atmospheric moisture and aerosol content, regional albedo, altitude and local skylines are notably investigated. Results will be reported subsequently.

2. METHODS

2.1 *Background information on original model*

The Perez diffuse irradiance model incorporates two basic components. The first is a geometric de-

† Member ISES.

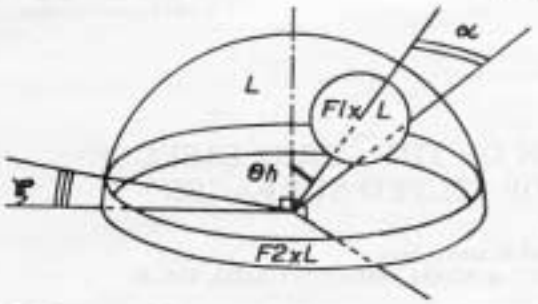

Fig. 1. Perez model's representation of the sky hemisphere

scription of the sky hemisphere superimposing a circumsolar disc and horizon band on an isotropic background (Fig. 1). This configuration was chosen to account for the two most consistent anisotropic effects in the atmosphere: Forward scattering by aerosols and multiple Rayleigh scattering and retroscattering near the horizon. Assuming that radiances in the circumsolar and horizon regions are, respectively, equal to F_1 and F_2 times that of the background, then the diffuse irradiance D_c, impinging on a plane of slope s, is obtained from the horizontal diffuse D_h using

$$D_c = D_h \left[\frac{0.5(1 + \cos(s)) + a(F_1 - 1) + b(F_2 - 1)}{1 + c(F_1 - 1) + d(F_2 - 1)}\right], \quad (1)$$

where a and b are the solid angles occupied, respectively, by the circumsolar region and the horizon band weighted by their average incidence on the slope. The parameters c and d are the equivalent of a and b for the horizontal. These are specified in the nomenclature.

The second component is empirical and establishes the value of the brightness coefficients F_1 and F_2 as a function of the insolation conditions. These conditions are parameterized by three quantities which describe, respectively, the position of the sun, the brightness of the sky dome, and its clearness. These quantities are, respectively, (1) the solar zenith angle Z; (2) the horizontal diffuse irradiance D_h; and (3) the parameter ϵ equal to the sum of D_h and direct normal I divided by D_h. It will be noted that these three quantities require no more input than is normally required by other models to compute hourly irradiance on a slope.

As an example of this parameterization, a scatter plot is presented in Fig. 2 which shows the distribution, in the (D_h, ϵ) plane at Z = constant of hourly observations recorded during a three-year period in Trappes and Carpentras, France[15]. In this figure, D_h has been normalized to extraterrestrial global and is referred to as "delta". This shows the dependent character of D_h and ϵ for high ϵ's (clear skies) and their independent nature for low ϵ's (overcast and partly cloudy cases).

For practical applications the (Z, D_h, ϵ) space was divided into 240 sky condition categories (5 for Z, 6 for D_h and 8 for ϵ). For each category, a pair of (F_1, F_2) coefficients was established. These coefficients were obtained from the least square fitting of eqn (1) to actual data recorded on sets of sloping pyranometers.

2.2 *Summary of changes from original to present model configuration*

The rationale behind each modification was to render the model less complex to use while either maintaining or improving its accuracy. This was judged by testing each version of the model against the three-year data sets from Trappes and Carpentras, France, including hourly global irradiance

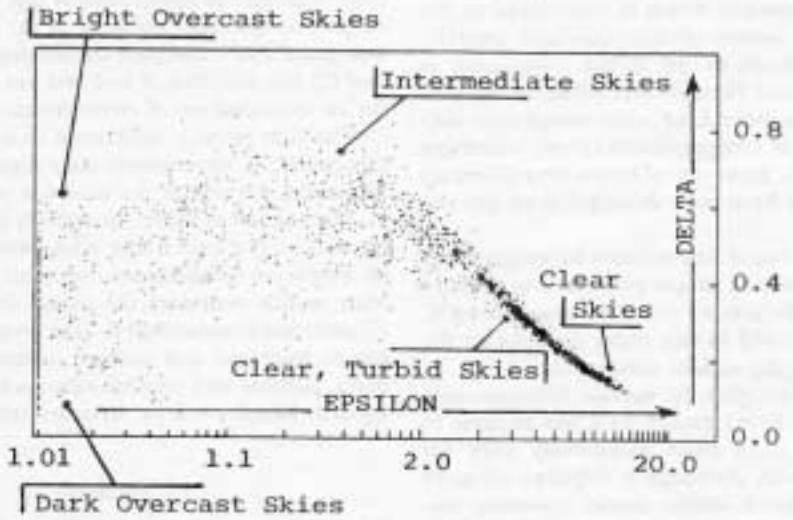

Fig. 2. Distribution of observed hourly events in Trappes and Carpentras (two years of data), in the D_h, ϵ plane for $Z \in [45°, 55°]$.

measurements on five tilted surfaces. The results of these tests are presented in the next section.

2.2.1 *Use of reduced brightness coefficients.* An important drawback of eqn (1) is its non-linearity with respect to F_1 and F_2 as defined earlier. The determination of these coefficients through least square fitting calls notably for a series of approximations and for solving sets of non-linear equations which may require considerable computation.

A major step toward simplification was taken by rewriting the model's governing equation using redefined brightness coefficients. Equation (1) may be written as [16]

$$D_c = D_h \left(\frac{D_c^i + D_c^c + D_c^h}{D_h^i + D_h^c + D_h^h} \right), \quad (2)$$

where the superscripts i, c and h refer, respectively, to the diffuse contribution, on the horizontal or the slope, of the isotropic background of the circumsolar and the horizon regions. Noting that the denominator of the right-hand side of eqn (2) is equal to D_h, this may be written as

$$D_c = D_h \left(\frac{D_c^i}{D_h} + \frac{D_c^c D_h^c}{D_h D_h^c} + \frac{D_c^h D_h^h}{D_h D_h^h} \right). \quad (3)$$

Further, one notes that D_c^c/D_h^c equal to a/c, that D_c^h/D_h^h is equal to b/d and that D_c^i is, by definition, given by

$$D_c^i = 0.5\,(1 + \cos(s))\,(D_h - D_h^c - D_h^h). \quad (4)$$

Finally, if D_h^c/D_h is set equal to F_1^i and D_h^h/D_h to F_2^i, eqn (3) becomes

$$D_c = D_h[0.5(1 + \cos(s))\,(1 - F_1^i - F_2^i) + F_1^i(a/c) + F_2^i(b/d)]. \quad (5)$$

Equation (5) is linear with respect to the terms F_1^i and F_2^i defined as reduced brightness coefficients. Conceptually they represent the respective normalized contributions of the circumsolar and horizon regions to the total diffuse energy received on the horizontal, whereas the original coefficients represent the increase in radiance over the background in both regions. For instance, a value of 0.5 for F_1^i indicates that 50% of horizontal diffuse behaves approximately as direct radiation, whereas a value of F_2^i equal to 0.2 indicates that a vertical surface will access an additional amount of energy equal to 20% of the horizontal diffuse radiation.

The relationship between the reduced coefficients and the original ones are the following:

$$F_1^i = c(F_1 - 1)/[1 + c(F_1 - 1) + d(F_2 - 1)], \quad (6)$$

$$F_2^i = d(F_2 - 1)/[1 + c(F_1 - 1) + d(F_2 - 1)]. \quad (7)$$

It will be noted that eqns (5) and (1) define exactly the same model framework. As before, the new coefficients may be derived empirically from experimental data recorded on sloping surfaces.

2.2.2 *Allowance for negative coefficients.* In its original setup the model did not allow for coefficients smaller than one (i.e. negative reduced coefficients). In other words the model returned to an isotropic configuration whenever observations could not be explained by an increase in radiance in either of the anisotropic regions. This setup explained most situations except overcast occurrences when the top of the sky dome is the brightest region[17].

Although negative coefficients are physically meaningless (since by definition this would mean negative energy received from a region in the dome), the use of negative F_2^i coefficients is equivalent, as far as flat plate surfaces are concerned, to adding a third brighter region at the top of the sky hemisphere. This new setup yields noticeable performance improvements particularly for climates where cloudy conditions prevail.

2.2.3 *Geometric framework modifications.* (a) *Horizon band*: The original configuration called for a 6.5° elevation horizon band. A rigorous definition of the term b in eqn (1) or (5) is rendered complex by such assumption. This was partly circumvented in the original model by accounting only for the half horizon band facing the slope, thus causing a discontinuity between the horizontal and slopes approaching 0°.

A much simpler configuration is now proposed whereby all the energy of the horizon band is contained in an infinitesimally thin region at 0° elevation. Equation (5) becomes

$$D_c = D_h[0.5(1 + \cos(s))\,(1 - F_1^i) + F_1^i(a/c) + F_2^i \sin(s)]. \quad (8)$$

(b) *Circumsolar region*: The circumsolar region was originally set at 15° half angle. A much simpler approach would be to assume that all circumsolar energy originates from a point source; In this case eqn (8) may be simply written as follows:

$$D_c = D_h[0.5(1 + \cos(s))\,(1 - F_1^i) + F_1^i(\cos(\theta_c)/\cos(Z)) + F_2 \sin(s)]. \quad (9)$$

However, unlike for the horizon band, this simplification causes small performance deterioration, noticeable for the non-south orientations—for which low sun incidence events and therefore the physical size of the circumsolar region have a larger impact. A 25° half-angle circumsolar region was found to provide the best overall performance and is used as a basis to illustrate the impact of the other simplifications and changes described hereafter. The 0° point source option will be proposed as an alternative version of this model. Its operational configuration is reported in Section 3. For infor-

mation, performance validation results using the model with 35°, 25°, 15° and point source circumsolar regions are presented in Table 5.

It is important at this point to remind the reader that the circumsolar representation used in this model (fixed width, homogeneous circular zone) is acceptable only for collecting elements with wide field of view (e.g. flat plate collectors). It would be inaccurate to use this representation as is to compute radiance (or luminance) in specific points of the sky dome. This would require a more detailed description of the forward scattered radiation, accounting for actual radiance profiles and for their variations with insolation conditions (e.g. see [18]). The same is true for the horizon brightening representation used in this model. An expanded version of the model, suited for such applications, is currently under development.

2.2.4 *Optimization of insolation parameterization.*

(a) *Replacement of D_h by Δ*: The second quantity selected to describe insolation conditions (horizontal diffuse irradiance, D_h) is not totally independent from the first quantity (solar zenith angle). Independence between these two dimensions describing, respectively, the position of the sun and the brightness of the sky may be achieved by selecting a new second dimension, Δ, defined as

$$\Delta = (D_h m)/I_0,$$

where m is the relative air mass and I_0 the extraterrestrial radiation. Normalization with respect to I_0 also renders this dimension independent of the users' unit.

(b) *Redefinition of the Δ, ϵ, Z grid*: The discrete sky condition 3D space associated with the original model is composed of 240 categories.

Each of these specifies a pair of coefficients. This approach was chosen primarily to facilitate observational analysis of experimental data. It has the advantage of requiring no computation for querying F_1' and F_2' for a given sky condition; however, the user must carry a table of 480 terms.

An alternate approach would consist of using analytical functions for F_1' and F_2'. Although simpler in concept, the fully analytical approach was rejected because of the added computational time caused by a rather complex formulation. This complexity is due mostly to the variable ϵ which requires a five degree polynomial (i.e. a 24 term expression if the variations with Δ and Z are assumed linear) to approach the precision of the original grid-based approach.

A compromise is proposed here, whereby F_1' and F_2' are expressed as analytic functions of Δ and Z while an eight-category discrete axis is kept for ϵ. The partition of that axis is optimized to provide the same mean variation of F_1' and F_2' in each category, based on the four-year experimental data set pooled from the two French sites. The analytic function in each ϵ category is of the form $e + fZ + g\Delta$, where e, f, g are constants. Indeed, variations with Z and Δ are found to be well-explained by independent linear approximations.

3. RESULTS

3.1 *New model formulation*

The new governing equation of the model is given in section 2.2.3. [eqn (8)]. All terms were defined above and are summarized in the nomenclature. The reduced coefficients $F_1'(Z, \Delta, \epsilon)$ and $F_2'(Z, \Delta, \epsilon)$ are given in Table 1. A simpler, slightly less accurate version of this new model [eqn (9)], is also introduced; the corresponding brightness coefficients are given in Table 2.

Scatter plots in Figs. 3, 4 and 5 illustrate the variations of F_1' and F_2' with respect to Z, Δ and ϵ, respectively. Variations with Z were plotted for ϵ values comprised between 2.5 and 5 corresponding to intermediate to clear and turbid skies. Variations with Δ were plotted for $\epsilon < 1.05$, that is, for overcast

Table 1. Generic circumsolar (F_1') and horizon brightening (F_2') coefficients developed from Trappes and Carpentras data for the 25° circumsolar model

ϵ bin #	Upper limit	Cases^ (%)	25° circumsolar region F_{11}'	F_{12}'	F_{13}'	F_{21}'	F_{22}'	F_{23}'
1	1.056	24.8	−0.011	0.748	−0.080	−0.048	0.073	−0.024
2	1.253	9.32	−0.038	1.115	−0.109	−0.023	0.106	−0.037
3	1.586	7.17	0.166	0.909	−0.179	0.062	−0.021	−0.050
4	2.134	7.88	0.419	0.646	−0.262	0.140	−0.167	−0.042
5	3.230	10.85	0.710	0.025	−0.290	0.243	−0.511	−0.004
6	5.980	18.57	0.857	−0.370	−0.279	0.267	−0.792	0.076
7	10.080	15.17	0.734	−0.073	−0.228	0.231	−1.180	0.199
8	—	6.96	0.421	−0.661	0.097	0.119	−2.125	0.446

$$F_1' = F_{11}'(\epsilon) + F_{12}'(\epsilon)^*\Delta + F_{13}'(\epsilon)^*Z$$
$$F_2' = F_{21}'(\epsilon) + F_{22}'(\epsilon)^*\Delta + F_{23}'(\epsilon)^*Z$$

^ Percent of total cases for 2 years each of Trappes and Carpentras, France.

Table 2. Generic circumsolar (F_1') and horizon brightening (F_2') coefficients developed from Trappes and Carpentras data for the point source circumsolar model

ϵ bin #	Upper limit	Cases^ (%)	Point source circumsolar region					
			F_{11}'	F_{12}'	F_{13}'	F_{21}'	F_{22}'	F_{23}'
1	1.056	24.08	0.041	0.621	−0.105	−0.040	0.074	−0.031
2	1.253	9.32	0.054	0.966	−0.166	−0.016	0.114	−0.045
3	1.586	7.17	0.227	0.866	−0.250	0.069	−0.002	−0.062
4	2.134	7.88	0.486	0.670	−0.373	0.148	−0.137	−0.056
5	3.230	10.85	0.819	0.106	−0.465	0.268	−0.497	−0.029
6	5.980	18.57	1.020	−0.260	−0.514	0.306	−0.804	0.046
7	10.080	15.17	1.009	−0.708	−0.433	0.287	−1.286	0.166
8	—	6.96	0.936	−1.121	−0.352	0.226	−2.449	0.383

$$F_1' = F_{11}'(\epsilon) + F_{12}'(\epsilon)^*\Delta + F_{13}'(\epsilon)^*Z$$
$$F_2' = F_{21}'(\epsilon) + F_{22}'(\epsilon)^*\Delta + F_{23}'(\epsilon)^*Z$$

^ Percent of total events for 2 years each of Trappes and Carpentras, France

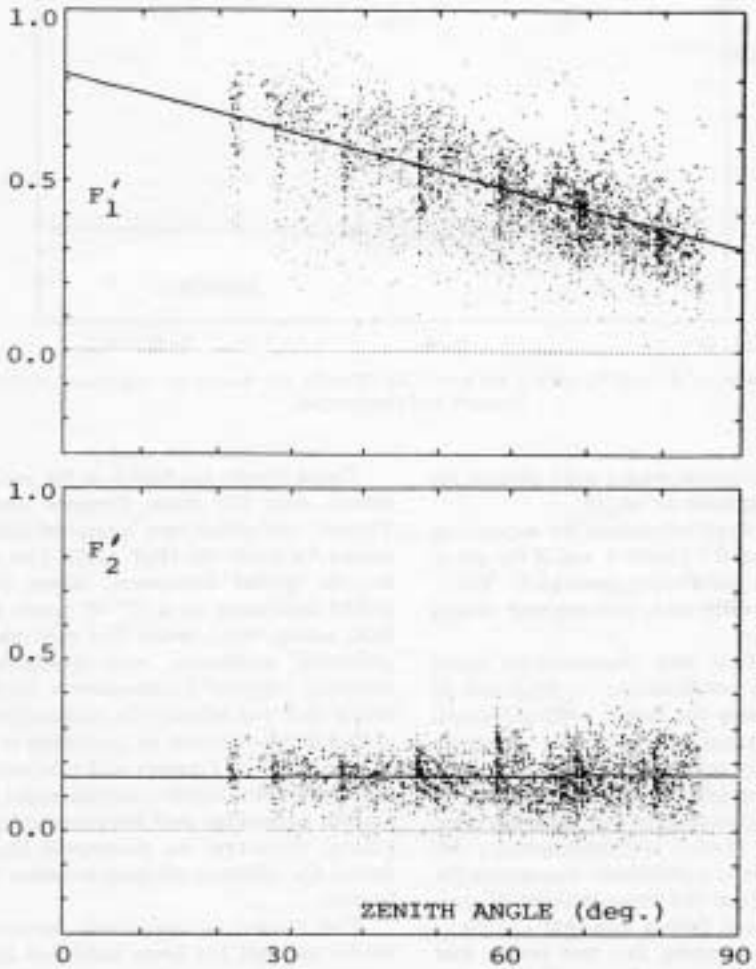

Fig. 3. Variations of F_1' and F_2' with solar zenith angle for $\epsilon \in [2.5, 5]$. Results based on two years of data from Trappes and Carpentras.

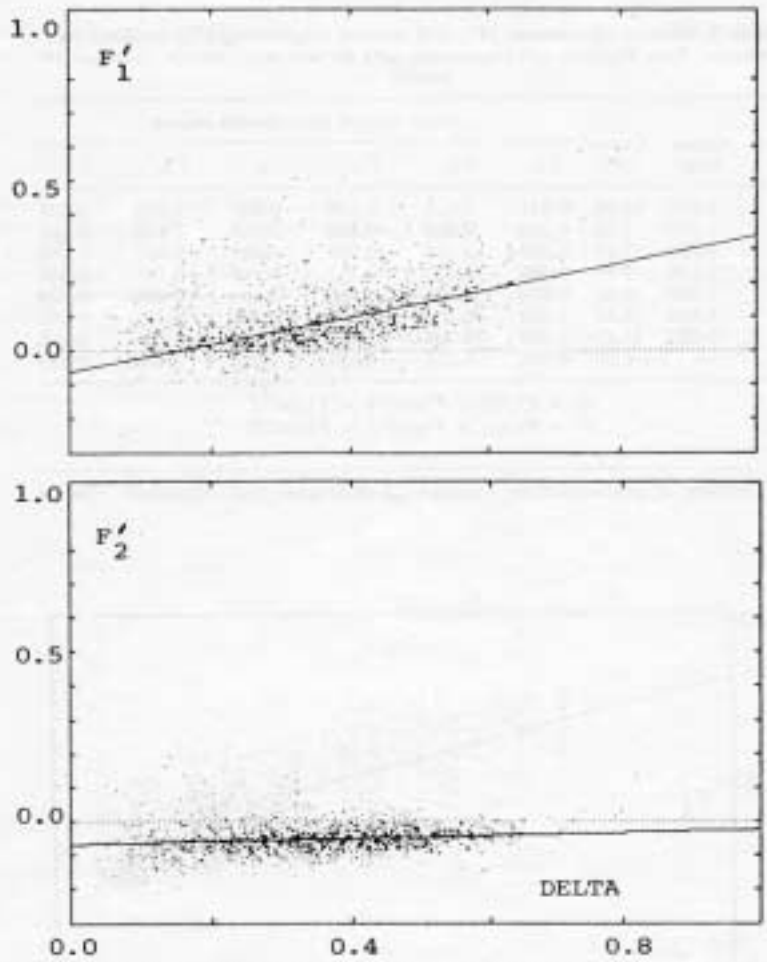

Fig. 4. Variations of F_1' and F_2' with Δ for $\epsilon < 1.05$. Results are based on two years of data from Trappes and Carpentras.

conditions, while variations with ϵ were plotted for zenith angles ranging from 45° to 55°.

The use of linear approximations for explaining the variations of F_1' and F_2' with Δ and Z for given ϵ intervals are clearly justified by these plots. Variations with ϵ are more difficult to express with simple analytic expressions.

These plots confirm past observations made about the brightness coefficients: (1) evidence of circumsolar brightening for bright overcast skies; (2) maximum of circumsolar brightening for partly cloudy to clear highly turbid atmospheres; (3) decrease of circumsolar brightening and marked increase of horizon brightening for low turbidity clear skies; (4) fairly low scatter in experimentally derived F_1' and F_2'—this is particularly interesting for intermediate skies given the large number of possible sky configurations falling into that category. It will be noted, concerning this last point, that much of the dispersion for $\epsilon < 2$, (see Fig. 5), may be explained by variations of Δ.

These results are based on the analysis of a composite data file from Trappes and Carpentras, France, including two years of hourly measurements for each site (Ref. [12]). The measurements include global irradiance, direct irradiance and global irradiance on a 45° tilt south plane and vertical south, west, north and east planes. Ground-reflected irradiance was available from sky-shielded vertical pyranometers facing north and south and was effectively removed from the tilted global measurements as described in [10].

The sites of Trappes and Carpentras represent two different climatic environments (respectively, marine temperate and Mediterranean). They constitute, therefore, an acceptable basis to use the model for climates ranging between these two extremes.

The reader is cautioned, however, that this model has not yet been validated for all possible solar environments. An active program is now underway[14] which will either validate existing for-

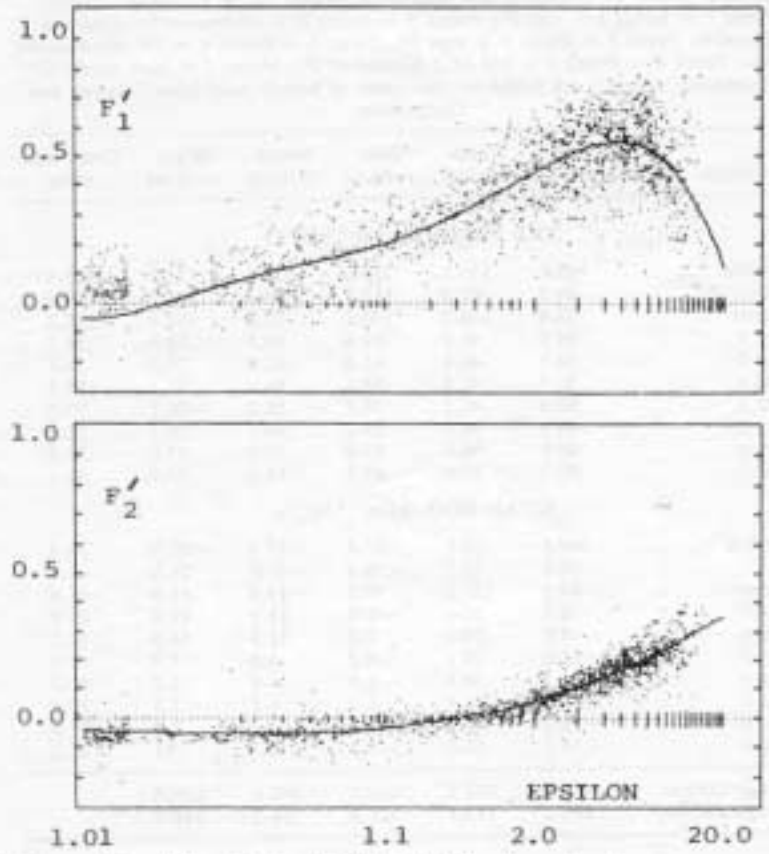

Fig. 5. Variations of F_1' and F_2' with ϵ for $Z \in [45°, 55°]$. Results are based on two years of data from Trappes and Carpentras.

mulations or provide sets of coefficients applicable to several key environments in the United States. This program investigates in particular the effects of altitude, regional albedo and seasonal local aerosol content on model configuration and performance.

3.2 *Model performance validation*

The value of the changes to the Perez model is considered from two perspectives. First, we examine the objective performance improvement in predicting diffuse radiation on sloping surfaces, and second, we examine the practical gain in terms of usability of the simplified model.

3.2.1 *Predictive performance-test results.* The main criteria used for model evaluation are the RMS and mean bias errors resulting from the actual and modeled diffuse. Test data are identical to that used to establish the coefficients, that is, two years of hourly data from both Trappes and Carpentras. In this respect the test of the Perez model may not be considered as independent. However, the pool of data is so large and the climates of the two sites so different that tests may be held as valid given the present status of knowledge in this area. More information on this aspect of the model will be obtained when SNL data becomes available for analysis[14].

Testing the model is a two-step process. First, the coefficients F_1 and F_2 must be generated. During this step, we may also observe the distribution of events with ϵ to optimize partitioning. Second, using the coefficients so generated, the model is used to calculate hourly radiation impinging on various surfaces. The errors generated are compared to three widely used models for reference. These are the isotropic[2], the Hay[3] and Klucher[4] models.

The Perez model has been tested at each step of the simplification discussed above. These results, based on Trappes and Carpentras data, are summarized in Table 3. Further, the original and the new model configurations' performances are compared for Albany, NY. Results are reported in Table 4. This is based on two years of SEMRTS hourly data[19].

The line labelled "Perez 1" is the original version of the model. Perez 2 through 7 are successive changes introduced in the model. The first step toward simplification is the introduction of a simpler governing equation (Perez 2). Note the slight loss

Table 3. Model performance test statistical results. Perez 1: original model; Perez 2 = Perez 1 + eqn (5); Perez 3 = Perez 2 + allowance for negative coefficients; Perez 4 = Perez 3 + eqn (8); Perez 5 = Perez 4 + 25° circumsolar region; Perez 6 = Perez 5 + use of Δ instead of D_h; Perez 7 = new model (25° circumsolar). Results are based on two years of hourly data from Trappes and Carpentras

Model	South 45°	North vertical	East vertical	South vertical	West vertical	Composite error
			RMS ERRORS ($kJ.m^{-2}.hr^{-1}$)			
Isotropic	163.1	119.8	159.0	155.4	151.0	150.4
Hay	94.3	87.9	112.7	98.4	101.7	99.3
Klucher	78.4	178.2	140.2	92.8	141.7	131.3
Perez 1	49.9	46.7	61.8	60.7	59.6	56.1
Perez 2	50.5	46.4	61.3	61.4	59.3	56.1
Perez 3	50.5	42.8	59.6	58.4	57.3	54.1
Perez 4	50.0	43.1	59.5	58.2	56.8	53.9
Perez 5	49.9	40.0	59.2	56.7	56.1	52.8
Perez 6	48.9	38.6	57.8	55.3	53.6	51.3
Perez 7	49.3	37.9	57.5	55.6	52.9	51.1
			MEAN BIAS ($kJ.m^{-2}.hr^{-1}$)			
Isotropic	−109.8	69.9	−37.4	−85.0	−27.5	72.5
Hay	−60.6	10.3	−38.9	−49.6	−26.9	41.2
Klucher	−39.1	121.1	30.6	−11.8	41.6	61.6
Perez 1	−8.5	24.4	−0.8	11.1	13.2	13.9
Perez 2	−8.6	25.1	0.8	11.8	14.3	14.5
Perez 3	−13.0	18.1	−6.2	4.8	7.3	11.1
Perez 4	−11.1	18.5	−6.5	3.8	7.0	10.7
Perez 5	−12.6	17.4	−6.3	6.1	7.5	10.9
Perez 6	−13.3	17.5	−5.8	5.5	7.9	11.0
Perez 7	−14.1	17.6	−6.5	4.7	7.1	11.2
Average Global	1369.2	232.5	619.1	848.6	610.6	
Average Diffuse	593.3	213.3	320.6	368.2	310.7	

Table 4. Model performance test statistical results for Albany, New York. Results are based on two years of hourly data

Model	South 43°	North vertical	East vertical	South vertical	West vertical	Composite error
			RMS ERRORS ($kJ.m^{-2}.hr^{-1}$)			
Isotropic	115.4	104.7	143.6	103.5	152.1	125.5
Hay	74.1	84.2	96.2	75.9	102.1	87.2
Klucher	51.2	158.4	134.2	79.5	141.7	120.1
Original Perez	40.8	36.3	55.1	68.8	63.2	54.3
New Perez *	39.9	31.5	53.2	61.9	60.0	50.7
New Perez ˚	41.2	28.1	50.3	61.3	57.3	49.1
			MEAN BIAS ($kJ.m^{-2}.hr^{-1}$)			
Isotropic	−72.5	56.5	−23.7	−36.2	−18.4	46.2
Hay	−32.4	2.2	−31.6	−9.6	−23.9	23.3
Klucher	−12.3	102.3	35.0	27.8	41.7	53.6
Original Perez	4.1	14.6	−4.2	31.6	6.6	16.0
New Perez *	−3.6	5.8	−15.3	18.0	−4.4	11.2
New Perez ˚	−5.5	4.6	−15.0	19.7	−4.2	11.8
Average Global	1350.4	233.9	584.4	794.5	579.6	
Average Diffuse	550.1	219.3	299.5	312.0	294.3	

* point source circumsolar; ˚ 25° circumsolar region

on south surfaces. This loss seems a reasonable trade-off with the much simpler model equation.

Step 3 reflects the allowance for negative coefficients. The table of mean bias errors emphasizes the importance of this step. The RMS errors also experience a considerable benefit from this simple change. It will be noted that all performance gains from negative coefficients results from better handling of overcast conditions.

Another simplifying change in the model is the reduction of the physical horizon band to a linear quantity. In addition to greatly simplifying model implementation, this has also provided a small overall performance improvement as shown in Perez 4.

Setting the circumsolar half angle to 25 degrees, an increase from the original 15 degrees, provided the overall best results for the two test sites. This change is included in Perez 5—performance variations as a function of circumsolar region definition are also reported, for information, in Table 5. Another noticeable performance gain (Perez 6) resulted from the use of Δ instead of D_n.

The final change for this study is the consolidation of Δ and Z as functional components of the model coefficients, F_1 and F_2. This is a fairly large evolutionary step for the model, and a slight accuracy loss is encountered on the south surfaces while slightly improving overall performance. This last step also includes optimization of ϵ axis partitioning.

3.2.2 *Computational improvement.* In assessing the computational improvement of the model, we will consider two points. First, the issue of model complexity. The model should be easy to implement and use for personal computer applications. It should also be simple enough to allow hand calculations if necessary. Second, we address the generation of coefficients, F_1 and F_2. A research organization should be able to develop these coefficients locally, rather than depend on a generic set intended to satisfy a broad climate spectrum.

Determination of brightening coefficients for a given event: In the old version, F_1 and F_2 were each stored in a three-dimensional matrix of 240 elements. Obtaining F_1 and F_2 required a mapping of the continuous variables Δ, ϵ and z into this discrete space. On average, this would require eight comparisons for the mapping (2.5 for Δ, 3.5 for ϵ and 2 for Z), and two table readings.

For the new model, F_1 and F_2 are determined by two simple functions. We must still map ϵ to a discrete space requiring an average of 3.5 comparisons. Then, a total of six table look-up are required.

On a computer, the differences between the original and the new methods are negligible in terms of time: logically, the new method is much more straightforward. Both methods require initialization: the old needs two arrays of 240 elements each while the new needs six arrays of eight elements each. When computed by hand, or on a calculator, the user would probably read the values from a chart.

Model framework: The old model framework was a function of the type

$$R = (a + bF_1 + cF_2)/(1 + dF_1 + eF_2),$$

whereas the new model is a function of the type

$$R = a' + F_1 b' + F_2 c',$$

where a', b' and c' are all simple functions. Implementing the new model is far simpler than the old particularly if one uses the point source version. Although, the savings in computer time for a single run is probably not noticeable.

In general, the model has become simple enough that its use is practical under almost any circumstances.

Generation of Coefficients set: Most users will never need to generate coefficients for F_1 and F_2,

Table 5. Variations of model performance with size of circumsolar region. Results are based on two years of hourly data from Trappes and Carpentras

Circumsolar region sustaining half angle	South 45°	North vertical	East vertical	South vertical	West vertical	Composite error
			RMS ERRORS ($kJ.m^{-2}.hr^{-1}$)			
0°	49.3	43.8	61.8	57.6	56.0	54.1
15°	48.4	40.6	58.8	55.8	53.6	51.9
25°	49.2	37.9	57.4	55.5	52.8	51.0
35°	51.6	36.5	57.8	55.9	53.9	51.7
			MEAN BIAS ($kJ.m^{-2}.hr^{-1}$)			
0°	−10.4	19.3	−6.1	2.5	6.6	10.6
15°	−11.2	18.2	−6.7	3.3	6.5	10.5
25°	−14.0	17.6	−6.4	4.6	7.0	11.1
35°	−18.3	18.2	−4.0	8.0	8.8	12.9

as a well-rounded generic and/or environment-dependant set(s) will be made readily available[14]. However, research facilities with access to a solar data base may want to develop their own coefficients for a specific environment. This process is now greatly simplified. A program to solve a system of non-linear equations used to be required. This could consume considerable computing resources, and could generate non-converging solutions. Coefficient generations now involves only solving sets of linear equations.

4. CONCLUSIONS

A summary of the modifications performed on the Perez model to increase its simplicity, while maintaining or improving accuracy has been presented. While the key assumptions defining the model remain unchanged, substantial "operating" modifications have made the model fairly simple to implement and use for microcomputer-based applications, well in line with other, less accurate models.

Together with increased simplicity, the proposed changes result in improved accuracy on all tested orientations and slopes. Improvements were found to be most noticeable for vertical surfaces particularly for the north-facing one. A simplified "point source" version of this new model is also proposed. It also features improved accuracy on the original model, but to a lesser degree for non-south surfaces.

Each simplification was validated based on two years of hourly data from Trappes and Carpentras, France: two environmentally distinct sites featuring, respectively, humid oceanic and dry Mediterranean climates. Conclusions reached for these two sites were substantiated with data from Albany, New York.

The generic models established for the two French sites now feature an improvement of approximately 2.5–3 to 1 over the isotropic model. RMS errors for all orientations are kept under 16 W m^{-2} while mean bias errors are kept under 5 W m^{-2} for the two sites tested.

It will finally be noted that the main focus of this paper was to introduce a simpler version of a model which has already been extensively validated. Further questions remain concerning the potential impact of altitude, regional/seasonal albedo and local atmospheric moisture and particulate content on the model configuration (i.e. intensities of horizon and circumsolar brightening) and on its performance. However, it is not thought, based on existing validations, that these should have such an effect as to drastically change the performance hierarchy (i.e. isotropic versus Hay versus Klucher versus Perez) shown in Table 3. These questions are currently being addressed and will be the object of upcoming communications.

Acknowledgements—This work was supported by Sandia National Laboratories under Contract No. 56-5434. Parallel work funded by New York State ERDA and previous work funded by SERI were helpful to the development of this research. The authors acknowledge the critical and constructive comments of A. Zelenka of the Swiss Meteorological Institute.

NOMENCLATURE

z Solar zenith angle
F_1 Original circumsolar brightness coefficient
F_2 Original horizon brightness coefficient
D_c Diffuse irradiance impinging on a tilted surface
D_h Diffuse irradiance on the horizontal
s Plane tilt angle
a Solid angle occupied by the circumsolar region, weighted by its average incidence on the slope. In this study a is approximated as follows:

$$a = 2(1 - \cos\alpha)\chi_c$$

where α is the circumsolar region half angle and χ_c is given by

$$\chi_c = \psi_h \cos\theta_c \text{ if } \theta_c < \pi/2 - \alpha,$$
$$\chi_c = \psi_h\psi_c \sin(\psi_c, \alpha)$$

if $\theta_c \in [\pi/2 \pm \alpha]$ and $\chi_c = 0$, otherwise, where θ_c is the incidence angle on the tilted plane, ψ_h is defined below (see term c) and $\psi_c = [(\pi/2 - \theta_c + \alpha)/\alpha]/2$

b Solid angle occupied by the horizon region, weighted by its average incidence on the slope. This is approximated as follows:

$$b = 2\xi/\pi \sin\xi',$$

where ξ is the angular thickness of the horizon band and ξ' is given by

$$\xi' = (\pi - \xi)/\pi + \xi/2$$

c Solid angle occupied by the circumsolar region, weighted by its average incidence on the horizontal. In this study, c is approximated as follows:

$$c = 2(1 - \cos\alpha)\chi_h,$$

where χ_h is given by

$\chi_h = \cos Z$ if $Z < \pi/2 - \alpha$,
$\chi_h = \psi_h \sin(\psi_h, \alpha)$, otherwise,
where ψ_h is given by
$\psi_h = (\pi/2 - z + \alpha)/2\alpha$ if $Z > \pi/2 - \alpha$
$\psi_h = 1$, otherwise

d Solid angle occupied by the horizon band weighted by its average incidence on the horizontal. d is given by

$$d = (1 - \cos 2\xi)/2$$

ϵ Sky clearness parameter given by

$$\epsilon = (D_h + I)/D_h,$$

where I is the direct normal incidence irradiance
Δ New sky brightness parameter given by

$$\Delta = D_h m/I_0$$

where m is the relative air mass and I_0 the normal incidence extraterrestrial radiation. (A constant value was used in this study.)

F_1 New circumsolar brightness coefficient

F_2 New horizon brightness coefficient

REFERENCES

1. R. R. Perez, J. T. Scott and R. Stewart, An anisotropic model for diffuse radiation incident on slopes of different orientations, and possible applications to CPCs. *Proc. of ASES*, Minneapolis, MN (1983), pp. 883–888.
2. D. Menicucci and J. Fernandez, Verification of photovoltaic system modeling codes based on system experimental data. *Proc. XVIIth IEE Photovoltaic Specialists Conference*, Kissimmee, FL (1984).
3. P. Ineichen, R. Perez and R. Seals, The importance of correct albedo determination for adequately modeling energy received by tilted surfaces. *Solar Energy* (in Press).
4. R. Perez and R. Stewart, Real time comparison of models estimating irradiation on sloping surfaces. *Proc. of ASES*, Anaheim, Ca. (1984).
5. B. Y. H. Liu and R. C. Jordan, The long-term average performance of flat-plate solar energy collectors. *Solar Energy* **7**, 53 (1963).
6. J. E. Hay and J. A. Davies, Calculation of the solar radiation incident on an inclined surface. *Proc. 1st Canadian Solar Radiation Data Workshop*, Toronto (1980) (Edited by J. E. Hay and T. K. Won), pp. 59–72.
7. T. M. Klucher, Evaluation of models to predict insolation on tilted surfaces. *Solar Energy* **23**, 111, 114 (1978).
8. M. H. Pepin-Bosc, D. Goetz and S. Janicot, Evaluation du rayonnement diffus du ciel. *Meteorologie et Energie Renouvelable Conference Proc.* AFME, Valbonne, France (1984).
9. R. Hulstrom and R. Bird, Solar irradiance available to various photovoltaic systems. Solar Energy Research Institute, Golden, CO, SERI/TI-215-2525 (1985).
10. R. Perez, R. Stewart, C. Arbogast, R. Seals and J. Scott, An anisotropic hourly diffuse radiation model for sloping surfaces—Description, performance validation, site dependency evaluation. *Solar Energy* **36**, 6 (1986).
11. International Energy Agency, Task IX, Subtask B, Solar Radiation Model Validation, Calculation of Solar Irradiances for Inclined Surfaces. Draft Report, IEA, Paris, France (1986).
12. B. Bourges, Analyse de Modeles de Calcul d'Eclairement Solaire sur Plans Inclines. Rapport CSTB—AR-MINES # 3.850.3168. Ecole des Mines de Paris, Paris, France (1985).
13. D. F. Menicucci, PVFORM Version 3.0, A photovoltaic system simulation program for stand-alone and grid-interactive applications. Sandia National Laboratories, Laboratories, Albuquerque, NM (1985).
14. Sandia National Laboratories Project #56-5434, SNL, Albuquerque, NM.
15. Direction de la Meteorologie, Service Meterologique Metropolitan, Stations #260 (Trappes) and 874 (Carpentras), Paris, France.
16. A. Zelenka, personal communication. Swiss Meteorological Institute, Zurich, Switzerland (1984).
17. CIE Committee E-3.2, Natural daylight—Official recommendations; 13th CIE Session Compte-Rendu, p. 11. Commission Internationale de l'Elairage, Paris, France (1955).
18. K. Coulson, *Solar and Terrestrial Radiation*, pp. 86–93. Academic Press, New York (1975).
19. USDOE Solar Energy Meteorology Research and Training Site, Region II, Albany, NY. Hourly data summaries, 1980–1981.